

## A study of the effect of iron island morphology and interface oxidation on the magnetic hysteresis of Fe-MgO (001) thin film composites

Steven R. Spurgeon, Jennifer D. Sloppy, Runzhe Tao, Robert F. Klie, Samuel E. Lofland et al.

Citation: *J. Appl. Phys.* **112**, 013905 (2012); doi: 10.1063/1.4730630

View online: <http://dx.doi.org/10.1063/1.4730630>

View Table of Contents: <http://jap.aip.org/resource/1/JAPIAU/v112/i1>

Published by the [American Institute of Physics](#).

---

### Related Articles

Chemical diffusion: Another factor affecting the magnetoresistance ratio in Ta/CoFeB/MgO/CoFeB/Ta magnetic tunnel junction

*Appl. Phys. Lett.* **101**, 012406 (2012)

Periodic arrays of magnetic nanostructures by depositing Co/Pt multilayers on the barrier layer of ordered anodic alumina templates

*Appl. Phys. Lett.* **101**, 013110 (2012)

Spin-polarized scanning tunneling microscopy study of Mn/Co/Cu(001) using a bulk Fe ring probe

*Appl. Phys. Lett.* **101**, 012404 (2012)

Isothermal switching of perpendicular exchange bias by pulsed high magnetic field

*Appl. Phys. Lett.* **100**, 262413 (2012)

Changes in magnetic properties of Co/Pd multilayers induced by hydrogen absorption

*J. Appl. Phys.* **111**, 123919 (2012)

---

### Additional information on J. Appl. Phys.

Journal Homepage: <http://jap.aip.org/>

Journal Information: [http://jap.aip.org/about/about\\_the\\_journal](http://jap.aip.org/about/about_the_journal)

Top downloads: [http://jap.aip.org/features/most\\_downloaded](http://jap.aip.org/features/most_downloaded)

Information for Authors: <http://jap.aip.org/authors>

## ADVERTISEMENT



Special Topic Section:  
**PHYSICS OF CANCER**

Why cancer? Why physics? [View Articles Now](#)

## A study of the effect of iron island morphology and interface oxidation on the magnetic hysteresis of Fe-MgO (001) thin film composites

Steven R. Spurgeon,<sup>1</sup> Jennifer D. Sloppy,<sup>1</sup> Runzhe Tao,<sup>2</sup> Robert F. Klie,<sup>2</sup> Samuel E. Lofland,<sup>3</sup> Jon K. Baldwin,<sup>4</sup> Amit Misra,<sup>4</sup> and Mitra L. Taheri<sup>1,a)</sup>

<sup>1</sup>*Department of Materials Science and Engineering, Drexel University, Philadelphia, Pennsylvania 19104, USA*

<sup>2</sup>*Department of Physics, University of Illinois at Chicago, Chicago, Illinois 60607, USA*

<sup>3</sup>*Department of Physics and Astronomy, Rowan University, Glassboro, New Jersey 08028, USA*

<sup>4</sup>*Center for Integrated Nanotechnologies, Los Alamos National Laboratory, Los Alamos, New Mexico 87545, USA*

(Received 20 February 2012; accepted 23 May 2012; published online 5 July 2012)

Fe-MgO tunnel junctions have received much attention for their use in hard drive read heads and other spintronic applications. The system is particularly interesting because of its magnetoresistive behavior and the abundance and low cost of its constituent elements. However, many questions remain about how the structure and chemistry of the Fe-MgO interface mediates magnetic behavior. In this study, we report on transmission electron microscopy, electron energy loss spectroscopy, and magnetic characterization of Fe-MgO composite films with various morphologies. We explore relationships between film morphology, intermixing, and the resulting effects on magnetic structure. We find the presence of oxidation at the Fe-MgO interface, with a detrimental impact on the saturation magnetization of the composite. We also observe changes in coercivity and magnetocrystalline anisotropy with film morphology and thickness. These results will inform the design of MgO-based tunnel junctions and improve our understanding of how processing conditions, resulting in morphological and chemical changes such as oxidation, affect magnetization. © 2012 American Institute of Physics. [<http://dx.doi.org/10.1063/1.4730630>]

### I. INTRODUCTION

The Fe-MgO system has been widely studied for its low-dimensional magnetic behavior, as well as its potential use in magnetoresistive tunnel junctions for memory applications. A small lattice mismatch of  $\sim 3.5\%$  upon a  $45^\circ$  in-plane rotation of the Fe lattice enables the growth of high-quality films according to the Fe (001)[110] || MgO (001)[100] orientation relationship.<sup>1-3</sup> By varying the deposition temperature and rate, it is possible to grow a wide range of Fe film morphologies, ranging from discrete islands to connected structures and continuous films.<sup>4</sup> Many studies have focused on an enhancement of magnetization in ultrathin Fe films, as well as magnetoresistive behavior in Fe-MgO-Fe tunnel junctions.<sup>5-8</sup> More recently the Fe-MgO system has been used as a canvas to explore relationships between microstructure and magnetism for potential device applications.<sup>9-12</sup>

It is known that Fe island coverage and interconnectivity can introduce configurational magnetic anisotropy that dominates over magnetocrystalline anisotropy.<sup>13</sup> This results in a rounding of hysteresis loops, which depends on island size and distribution, interfacial strain, and intermixing at the Fe and MgO interface.<sup>14</sup> There has also been much debate about the potential formation of an interfacial iron oxide layer and its effect on magnetic order.<sup>15-17</sup> Tunnel barrier oxide thickness and composition are crucial design parameters in mag-

netic tunnel junctions: a competing iron oxide layer could increase the magnetoresistance of the junction to unusable levels and lead to unpredictable device behavior.<sup>18,19</sup> Likewise, the presence of interface defects or intermixing can change the transport behavior of the junction.<sup>20</sup> Electron microscopy is an ideal probe of the Fe-MgO interface, enabling simultaneous high-resolution characterization of chemistry and structure. The use of transmission electron microscopy (TEM) and electron energy loss spectroscopy (EELS) makes it possible to identify the presence of any significant oxide layers while also exploring the effect of growth parameters on interdiffusion, roughness, and Fe film morphology. These measurements can then be correlated with changes in magnetocrystalline anisotropy measured by bulk magnetometry. This combination of techniques offers an improved understanding of the processing-property relationships necessary for the design of MgO-based spintronics.

### II. EXPERIMENTAL METHODS

Fe-MgO samples were first synthesized by electron beam deposition and were then characterized by a combination of structural and magnetic analyses. X-ray diffraction, electron microscopy, and spectroscopy were used to confirm the crystallinity and local structure of the films.

Commercial  $1 \times 1 \text{ cm}^2$  square MgO (001) substrates purchased from MTI International were annealed for 12 h at  $300^\circ\text{C}$  in a vacuum chamber at a base pressure of  $\sim 10^{-7}$  Torr. Fe films of three thicknesses (10, 20, and 30 nm) were then electron beam deposited at  $500^\circ\text{C}$  at a rate

<sup>a)</sup>Author to whom correspondence should be addressed. Electronic mail: [mtaheri@coe.drexel.edu](mailto:mtaheri@coe.drexel.edu).

of 0.2 nm/s. Each film was subsequently capped in a nominal 5 nm layer of Au, deposited at 30 °C and a rate of 0.5 nm/s. X-ray diffraction and fluorescence measurements were performed on the samples to confirm the orientation, crystallinity, and thicknesses of the Fe films. Secondary electron scanning electron (SEM) micrographs were captured at 10 keV accelerating voltage with a FEI Strata DB235 dual-beam focused ion beam (FIB) system. Cross-sectional TEM samples were then prepared by a “lift out” technique on the same DB235 system operating between 5 and 10 keV ion beam current.<sup>21</sup> Sputter redeposition and damage were cleaned with a Fischione 1010 low-angle ion mill operating at 0.5–1.5 keV and 4°–6° incidence angle. Images were captured on a JEOL 2100 LaB<sub>6</sub> TEM operating at 200 keV.

Energy-dispersive x-ray spectroscopy (EDS) maps were subsequently collected in scanning transmission electron microscopy (STEM) mode on a JEOL 2010 F STEM/TEM operating at 200 keV with a convergence angle of 15 mrad and a collection angle of 28 mrad. STEM-EDS can provide the local chemical information needed to develop a qualitative understanding of diffusion and oxidation at the interface. The same system was used to measure electron energy loss (EELS) spectra at various points across the Fe-MgO interface. EELS enables quantification of the relative oxidation state of the Fe atoms across the interface region.<sup>22</sup> The background was removed and the energy was calibrated using the known position of the Fe  $L_3$  edge.  $L_3/L_2$  intensity ratios were calculated by taking the second derivative of the measured data and then integrating the positive areas under each peak. This method is independent of background removal and does not depend on the method used to determine the continuous  $L$  edge contribution.<sup>23</sup> Fe valences were estimated the values provided by Cosandey *et al.*<sup>23</sup>

In-plane magnetic hysteresis loop curves were measured on the as-deposited samples at 300 K along the Fe  $\langle 100 \rangle$  and  $\langle 110 \rangle$  directions with a Quantum Design vibrating sample magnetometer (VSM).

### III. RESULTS

Bright field cross-sectional TEM images reveal the Fe island structure and morphology in the films. Figure 1 shows TEM images along the MgO  $\langle 100 \rangle$ ,  $\langle 011 \rangle$ , and  $\langle 012 \rangle$  zone axes of the films, with Fe layer thickness increasing from top to bottom. At the smallest Fe film thickness (Figs. 1(a) and 1(b)) discrete islands ranging in thickness from 5 to 10 nm are clearly visible. The islands are spaced approximately 10 nm apart and appear to show faceting along their edges. A region of light contrast is visible between the bottom edge of the islands and the top of the MgO substrate.

As shown in Figures 1(c) and 1(d), the film thickness increases the islands begin to coarsen and exhibit the formation of small interconnecting regions. The nominal island thickness is 20 nm, with interconnecting regions approximately 5 nm thick and 10 nm wide. The faceting evidenced in the previous film remains, as does the band of light contrast below the islands, which appears thinner in the  $\langle 100 \rangle$  orientation compared to the  $\langle 120 \rangle$  orientation. The 30-nm film (Figs. 1(e) and 1(f)) consists of a 30-nm continuous Fe layer, capped by small Fe islands ranging in size from 5–10 nm. At this point the island caps show more rounded edges instead of the facets previously observed. The layer of light contrast at the Fe-MgO interface is not visible in these samples.

High-resolution cross-sectional TEM micrographs (see insets of Fig. 1) demonstrate the crystallinity of the Fe islands and MgO substrate, as well as the uniformity and smoothness of the interface. The islands themselves appear to be largely single-crystalline and faceted. The cross-sectional TEM micrographs are complemented by scanning electron micrographs that offer a two-dimensional plan view of the surface of the films. In Figure 2(a), the 10-nm Fe film appears to consist of discrete, equiaxed islands  $\sim 25$  nm in diameter. The 20-nm Fe film (Fig. 2(b)) exhibits coarsening, enhanced island coverage and elongation of the islands to  $\sim 80$  nm. The surface morphology of the  $\sim 30$ -nm

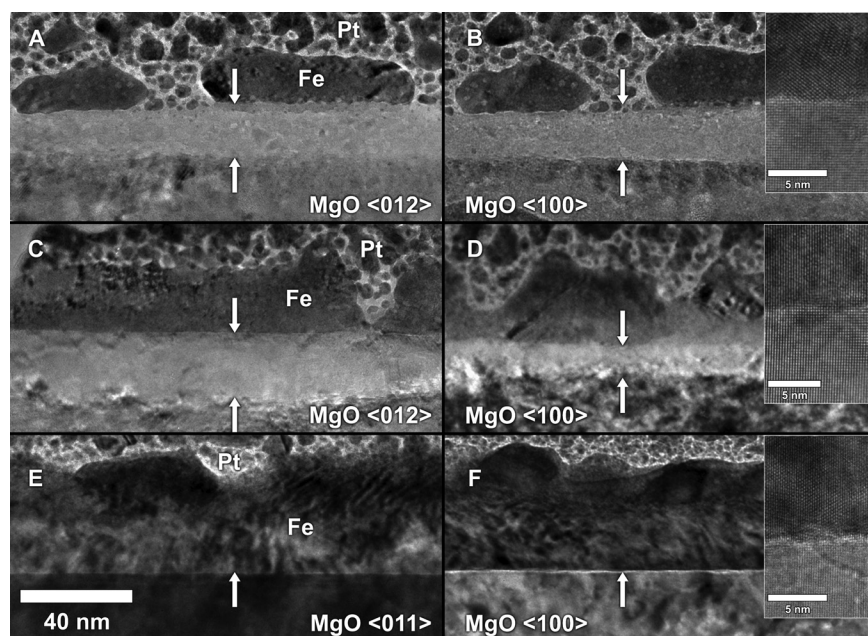


FIG. 1. Sequence of TEM bright field images illustrating the evolution of Fe island morphology and interconnectivity with increasing Fe thickness along MgO  $\langle 100 \rangle$ ,  $\langle 011 \rangle$ , and  $\langle 012 \rangle$  zone axes. (a), (b); (c), (d); and (e), (f) correspond to 10, 20, and 30 nm Fe thicknesses, respectively. Insets show high resolution images of each Fe-MgO interface and arrows indicate the boundaries of the Fe-MgO intermixed region.

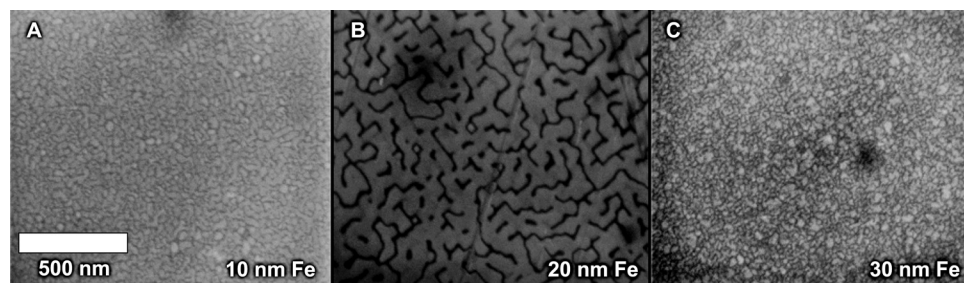


FIG. 2. SEM plan-view images illustrating the evolution of Fe island morphology with thickness. (a) Discrete, equiaxed islands. (b) Connected, anisotropic islands new layer of discrete, equiaxed islands.

Fe film (Fig. 1(c)) is similar to that of the 10-nm Fe film, consisting of equiaxed islands approximately 30 nm in diameter.

Figure 3 shows a bright field STEM-EDS image, as well as Fe *K* and Mg *K* edge maps for the 20-nm film. The bright field image displays the aforementioned band of light contrast between the Fe islands and the MgO substrate. The accompanying elemental maps show that this band is a transition region of intermixed Fe and Mg approximately 15 nm thick. This appears to indicate diffusion of Mg from the substrate into the Fe layer.

Previous EELS studies have shown that the strong Fe  $L_3$  and  $L_2$  white lines near 710 eV correspond to the transition of electrons from spin-orbit split levels  $2p_{3/2}$  and  $2p_{1/2}$  to unoccupied  $3d$  states.<sup>24,25</sup> The relative intensity of these two peaks is strongly dependent on the  $d$ -band occupancy and the Fe valence.<sup>26,27</sup> By measuring the  $L_3$  to  $L_2$  ratios at various points across the Fe-MgO interface, it is therefore possible to estimate the degree of oxidation. Since the magnetic properties of Fe depend on the  $3d$  occupancy, this information is essential for understanding the magnetic behavior of the composite.

The curves presented in Figure 1 are the sum of five spectra collected at each measurement point. Strong Fe  $L_3$  and  $L_2$  peaks are observed in the film layer away from the interface, as is expected. The ratio of these peaks corresponds to a Fe<sup>2+</sup> oxidation state (Fig. 4(b)). As the scan moves into the interface region, the intensity of these peaks begins to decay and their ratio changes, indicating a transition to a Fe<sup>~2.5+</sup> oxidation state. Approximately 8 nm into the transition region the Fe  $L_3$  and  $L_2$  peaks disappear, indicating the absence of Fe. This decrease in  $L_3$  and  $L_2$  intensity is accompanied by an increase in the intensity of the O *K* edge at ~537 eV, commensurate with the increasing oxygen content of the substrate. The *K* edge consists of a small prepeak at ~529 eV that decreases moving from spot 1–4 and indicates a transition from FeO to Fe<sub>2</sub>O<sub>3</sub>. The strong peak at ~537 eV is largely independent of the oxide phase but indi-

cates the presence of oxygen. Between spots 5–11 a broad peak also forms at ~557 eV that can arise from multiple-loss contributions.<sup>25</sup> These changes in the Fe *L* and O *K* edges appear to indicate both oxidation of the Fe layer and intermixing with the underlying MgO substrate.

Figure 5 shows hysteresis loops for the films measured along  $\langle 100 \rangle$  and  $\langle 110 \rangle$  Fe crystallographic directions. The Fe film volume was calculated x-ray fluorescence measurements for the various film thicknesses. The 10-nm and 20-nm films saturate at 1500 emu/cm<sup>3</sup>, while the 30-nm film saturates near 1800 emu/cm<sup>3</sup>. These values are close to the expected bulk saturation of 1700 emu/cm<sup>3</sup> but may differ due to oxidation at the interface and experimental error.<sup>28</sup> As shown in Figure 5(d), the coercivity increases from approximately ~238 Oe at 10 nm to ~428 Oe at 20 nm and decreases to ~55 Oe at 30 nm.

#### IV. DISCUSSION

The evolution of morphology and interface structure in these films can be measured by TEM and SEM micrographs. As shown in Figures 1(a) and 1(b), the thinnest 10-nm Fe film consists of discrete, faceted islands similar in size to those previously observed during growth at 500 °C.<sup>29</sup> Continuing growth transitions to a layer-by-layer mode, as supported by other studies.<sup>14,30</sup> This is supported by images of the 20-nm film, which show that the islands have started to connect into a uniform layer (Figs. 1(c) and 1(d)). For a thickness of 30-nm (Figs. 1(e) and 1(f)), there is a continuous Fe layer with some surface roughness. Because of the geometry of the sample, it is likely that the interconnectivity corresponds to the coarsening observed in SEM images (Fig. 2(b)). The increase in coverage at 20 nm also compares favorably to the minimum thickness for complete coverage predicted by helium atom scattering.<sup>31</sup> As growth continues the 30-nm film is again equiaxed with an average island size

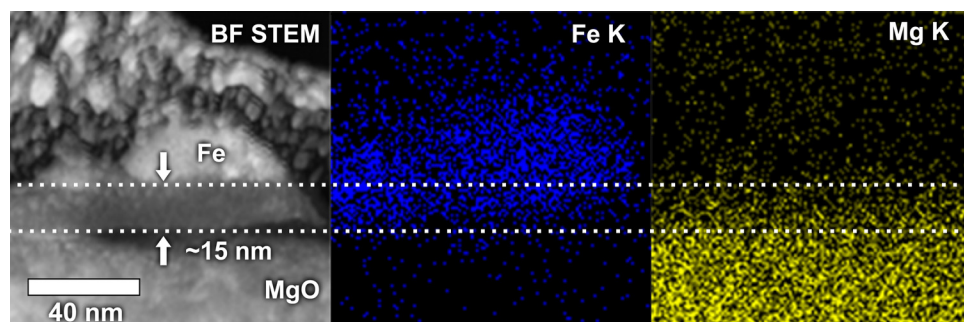


FIG. 3. STEM-EDS maps of the intermixing of a 20 nm Fe island and the MgO substrate. From left to right, a bright field STEM image, Fe *K* edge map, and Mg *K* edge map are shown. The region between the dashed lines corresponds to an intermixed interface layer.

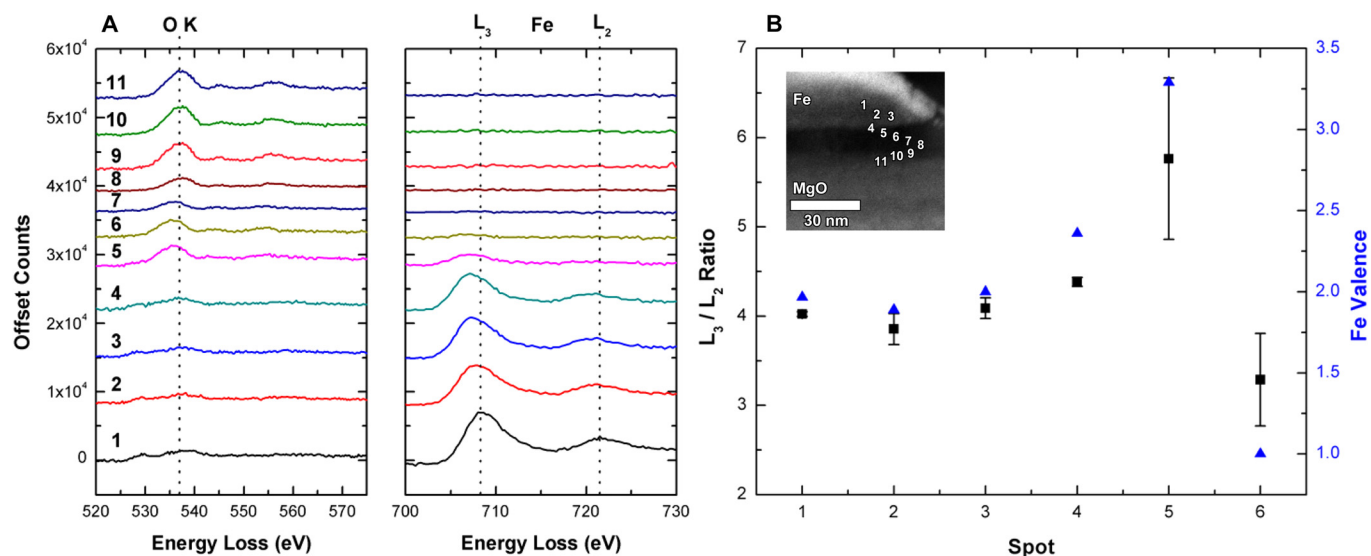


FIG. 4. STEM-EELS maps of the interface between a 20-nm Fe film and the MgO substrate. (a) A series of spectra collected across the intermixed region at the points labeled in the inset of (b). (b) The calculated Fe  $L_3/L_2$  peak ratios (squares) and the estimated Fe valence (triangles) from Cosandey *et al.*<sup>23</sup> Error bars correspond to the goodness of the Gaussian fit to the two peaks at each spot.

of 30 nm, corresponding to the formation of new Fe islands on a uniform sub-layer.

This behavior may be understood energetically using the model developed by Siegert and Plischke (S&P), which

employs Monte Carlo simulations to consider a diffusive current onto a substrate.<sup>32,33</sup> The authors find that Fe is expected to form pyramidal islands with  $\langle 011 \rangle$ -type facets in the initial stages of high-temperature growth. This faceting is

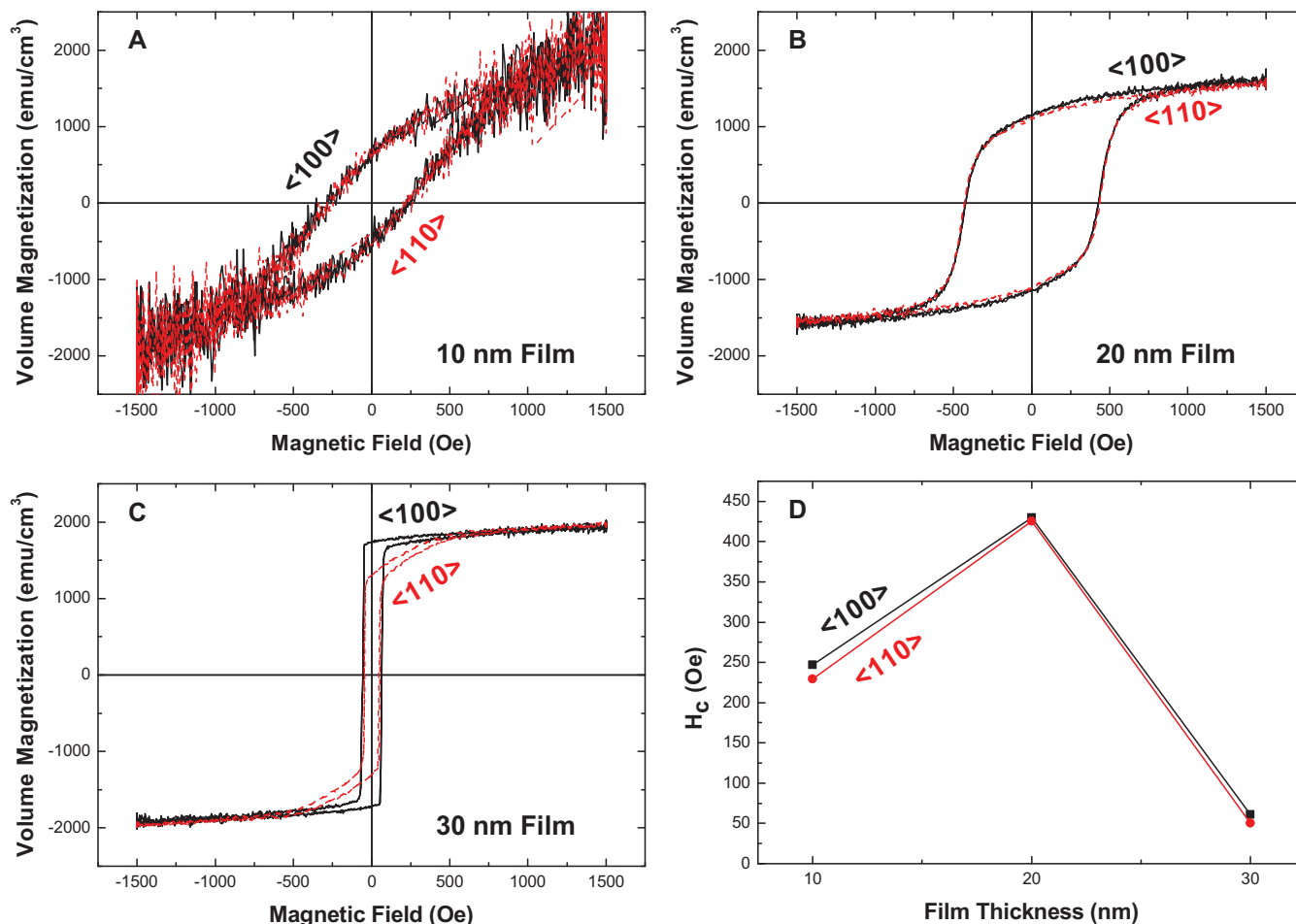


FIG. 5. In-plane magnetic hysteresis loops for 10, 20, and 30 nm Fe films ((a)–(c), respectively) along the Fe  $\langle 100 \rangle$  and  $\langle 110 \rangle$  directions. (a) splitting between the two directions, while in (c) an obvious anisotropy exists between the  $\langle 100 \rangle$  and  $\langle 110 \rangle$  directions. (d) Coercivities along  $\langle 100 \rangle$  and  $\langle 110 \rangle$  directions for each sample, with a peak at 20 nm.

seen in TEM micrographs of the thinner samples along the corners of the islands (Figs. 1(a) and 1(c)). In the S&P model, the faceted islands first nucleate on the free MgO surface and then coarsen according to a power law ( $t^{1/4}$ , where  $t$  = deposition time). Initial growth proceeds in an island growth mode due to the high surface energy of  $4.0 \text{ J/m}^2$  for Fe (001) compared to  $1.2 \text{ J/m}^2$  for MgO (001).<sup>34</sup> Island formation is preferred because of the high electronegativity difference between Fe and O, as well as a high cohesive energy and dielectric constant for MgO.<sup>31</sup> A relatively high monomer diffusion barrier of  $0.4 \text{ eV}$  has been calculated, which leads to a weak temperature dependence of adatom diffusion below  $\sim 220^\circ\text{C}$ . At low temperatures, adatoms are less mobile and these pyramidal structures remain stable even up to significant Fe thicknesses (200–300 nm).<sup>35</sup> For our high temperature depositions at  $500^\circ\text{C}$ , adatoms are able to overcome the barrier to surface diffusion and coalesce into a uniform layer. Our results are supported by helium atom scattering and infrared absorption studies that find that complete coverage is reached near 20 nm.<sup>31,36</sup>

The two thinner films exhibit a clear region of light contrast below the interface, a possible result of interdiffusion or oxidation. The diffusion of iron into the substrate is not unexpected at a  $500^\circ\text{C}$  deposition temperature.<sup>37,38</sup> A simple calculation of the expected diffusion length can be conducted, according to the diffusivity relationship  $\tilde{D} = 8.83 \exp\left(\frac{-74.6 \text{ kCal}}{RT}\right) \text{ cm}^2/\text{s}$  measured by other authors<sup>39,40</sup> where  $R$  is the ideal gas constant. Assuming that the diffusivity is largely independent of composition, we expect that the concentration profile will take the form  $C(x, t) = 1 - \text{erf}\left(\frac{x}{2\sqrt{\tilde{D}t}}\right)$ , where  $x$  is the depth normal to the interface and  $t$  the time. At the deposition temperature of  $500^\circ\text{C}$  and an approximate deposition time of 30 min, the concentration profile has an intermixed region of  $\sim 0.2 \text{ nm}$ . The diffusion length estimated by EELS from the drop off in the Fe white line signals is approximately 5–7 nm. The measured value is still an order of magnitude larger than the predicted diffusion length; a possible explanation is that the diffusivity values used in the above calculation were measured for bulk Fe powders and MgO single crystals while diffusivities are expected to be much larger in reactive thin film structures.

In addition to spatial information about diffusion, EELS allows one to study the migration of oxygen and oxidation of the Fe film at the interface. The oxidation state of the Fe away from the interface is  $\sim 2+$ , but approximately 4–5 nm into the transition region it increases to  $\sim 2.5+$ . This rise is accompanied by a rise in the intensity of the O  $K$  edge, indicating the possible formation of a mixed FeO-Fe<sub>2</sub>O<sub>3</sub> magnetite phase. The presence of this magnetite region could reduce the saturation magnetization of the film by an amount proportional to the oxidized volume. Assuming a saturation magnetization of  $1700 \text{ emu/cm}^3$  for bulk Fe and  $473 \text{ emu/cm}^3$  for Fe<sub>3</sub>O<sub>4</sub> and layer thicknesses of  $d_{\text{Fe}} \approx 16 \text{ nm}$  and  $d_{\text{Fe}_3\text{O}_4} \approx 4 \text{ nm}$ , we expect a saturation magnetization of  $\sim 1413 \text{ emu/cm}^3$ , close to the observed saturation of  $\sim 1500 \text{ emu/cm}^3$ .<sup>41</sup> Thus, EELS results indicate that oxidation could be a possible explanation for the film's reduced magnetization.

Magnetocrystalline anisotropy can be estimated from measured in-plane magnetic hysteresis loops. The work done  $W$  in the magnetization process is equal to the area encompassed by the  $M$ - $H$  loop,  $W = \int_0^M H dM$ . For cubic crystals we can define the anisotropy constants as follows:  $K_0 = W_{100}$  and  $K_1 = 4(W_{110} - W_{100})$ . Because these constants are based on relative changes in loop area, they should not be affected by differences in domain wall motion.<sup>28</sup> For the 20-nm film we estimate  $K_1 = 5.9 \times 10^5 \text{ erg/cm}^3$  and for the 30-nm film  $K_1 = 12 \times 10^5 \text{ erg/cm}^3$ . The measured value of  $5.9 \times 10^5 \text{ erg/cm}^3$  for the thinner film is on the same order of magnitude as bulk Fe ( $4.8 \times 10^5 \text{ erg/cm}^3$ , from Ref. 42) but the measured anisotropy for the thicker film is more than twice as large ( $12 \times 10^5 \text{ erg/cm}^3$ ). Martínez-Boubeta *et al.* have proposed that misfit energy introduced by dislocations can introduce an interface contribution to the anisotropy constant.<sup>14,43</sup> However, even the formation of misfit dislocations cannot account for the measured anisotropy value of the 30-nm film.

Other potential sources of anisotropy are interfacial roughness, intermixing, and oxidation of the Fe layer. While the films are relatively smooth, the latter two features have been observed by STEM-EDS and STEM-EELS. The formation of an iron oxide layer in particular could account for some of the observed changes in magnetocrystalline anisotropy. Previous studies of Co/Cu/Co/Fe<sub>3</sub>O<sub>4</sub>/MgO (001) spin valves have shown that the presence of the oxide layer can induce changes in coercivity and reorient the easy axis of the bottom Co layer.<sup>44</sup> Although the formation of an oxide layer is generally regarded as thermodynamically unfavorable, there have been conflicting reports about its synthesis.<sup>15,17,19</sup> Studies of CoFe<sub>2</sub>O<sub>4</sub> have shown significant diffusion of Mg into the oxide layer and a resultant reduction in saturation magnetization.<sup>45,46</sup> The transition from Fe<sup>2+</sup> to Fe<sup>2.5+</sup> observed in EELS may also be the result of the formation of a mixed valence magnetite phase. Because MgFe<sub>2</sub>O<sub>4</sub> is a thermodynamically stable spinel phase, its presence at the Fe-MgO interface cannot be entirely precluded.

Changes in the shape of the hysteresis loops may offer insight into the effects of film coverage on the magnetization process. The thinnest film (Fig. 5(a)) exhibits a rounded, sheared loop that progresses to a squarer loop for the 20-nm film (Fig. 5(b)) and finally a sharp, square loop at a thickness of 30 nm (Fig. 5(c)). The changes in loop shape correlate directly to changes in film morphology and thickness measured by SEM and TEM. Previous work has indicated that the rounding of hysteresis loops results from incomplete film coverage, as well as the introduction of configurational anisotropy from layer-by-layer (Vollmer-Weber) island growth.<sup>14</sup> The squaring of the hysteresis loops correlates to the observed increase in coverage. Likewise, the increasing presence of these anisotropy terms is further supported by a splitting in the  $\langle 100 \rangle$  and  $\langle 110 \rangle$  hysteresis loops: at 10-nm, the two loops are similar, but as the film thickness a clear distinction between the two develops. This magnetic behavior coincides with the transition from discrete islands to a uniform layer.

The observed changes in coercivity (Fig. 5(d)) can also be related to film morphology. The thinnest 10-nm film consists of discrete islands with a coercivity of  $\sim 238 \text{ Oe}$  that increases to  $\sim 428 \text{ Oe}$  at 20-nm as the islands begin to

connect. By 30-nm the islands have fully formed into a uniform layer and the coercivity drops to  $\sim 55$  Oe. Several effects resulting from the geometry of our samples may explain this behavior. It has been observed in thin film Co that  $H_C$  is highly dependent on coverage and film thickness.<sup>47,48</sup> Coercivity in Co rises with increasing film coverage but drops once a uniform layer has been formed. We see similar behavior during the transition from a discontinuous island network to a uniform film. This illustrates the importance of surface states and suggests that morphological barriers to domain wall motion can greatly affect coercivity. These conclusions are supported by modeling that predicts significant pinning and nucleation effects near island edges.<sup>49</sup> Studies of granular Fe thin films also confirm an enhancement of coercivity up to  $\sim 18$  nm grain size, followed by a decrease proportional to  $1/d$  (where  $d$  = film thickness).<sup>50</sup> It is thought that such grains possess a uniaxial surface anisotropy; as the surface/volume ratio decreases, the surface term becomes less dominant. This surface anisotropy may be responsible for suppression of superparamagnetic behavior, which would explain the increase in coercivity going from 30 to 20 nm.<sup>51</sup>

We may also consider local demagnetizing fields present near the island surfaces, which act to oppose the applied magnetic field.<sup>52</sup> Because the demagnetizing field depends on geometry and volume, the changing morphology and increasing thickness may affect  $H_C$  between 10 and 20-nm. Lastly, strain and local chemistry should not be neglected. It is known that the magnetostriction of Fe reverses sign near 20 nm, the result of strain effects with increasing thickness.<sup>53</sup> Similar strain effects have been observed in FeCo, with  $H_C$  attaining a peak near 30 nm and decreasing with increasing film thickness, the result of strain gradients that form during growth.<sup>54</sup> Interdiffusion between the film and substrate may also introduce additional pinning sites that compete with increasing film coverage.<sup>55</sup>

## V. CONCLUSIONS

Electron micrographs reveal a clear progression in Fe-film morphology as a function of thickness. Discrete islands coarsen and interconnect until a uniform layer is formed, upon which a second layer begins to grow. Cross-sectional TEM micrographs indicate that the islands are faceted and that the interface between the Fe film and MgO substrate is largely free of dislocations. EELS, and EDS maps show evidence for the intermixing of Fe and Mg at the interface and the formation of an interfacial iron oxide layer, which is consistent with the decreased saturation magnetization of some of the films. Measured changes in coercivity, magnetocrystalline anisotropy, and the squaring of the hysteresis loops are related to increases in island coverage and thickness. While the calculated anisotropy constants are on the same order of magnitude as the expected values, there is evidence that the values are also affected by oxidation of the Fe. We propose several mechanisms for the observed coercivity behavior and find a significant dependence on film morphology, consistent with models of domain wall pinning. Future studies with polarized neutron reflectometry, x-ray photoem-

ission spectroscopy, and EELS mapping of the films will make it possible to further quantify the magnetic and chemical nature of the interface with respect to film structure and morphology. These studies will be complemented by local TEM analysis to develop deterministic models of coercivity and hysteresis behavior.

## ACKNOWLEDGMENTS

The authors gratefully acknowledge support from the National Science Foundation under Grant #DGE-0654313 (M.L.T.), #CMMI-1031403 (M.L.T.), #DMR-0846784 (R.F.K., R.T.), #DMR-0908779 (S.E.L.), and #DMR-0821406 (S.E.L.), as well as from the Office of Naval Research under Grant #N00014-1101-0296/12PR02130-02 (M.L.T.). Electron microscopy was conducted in Drexel University's Centralized Research Facilities and at the Research Resources Center at the University of Illinois-Chicago; magnetic measurements were performed in Rowan University's Department of Physics and Astronomy. Author S.R.S. is supported by a National Science Foundation Integrative Graduate Education and Research Traineeship (IGERT) and a Department of Defense National Defense Science and Engineering Graduate (NDSEG) Fellowship.

<sup>1</sup>A. Di Bona, C. Giovanardi, and S. Valeri, "Growth and structure of Fe on MgO (001) studied by modulated electron emission," *Surf. Sci.* **498**(1), 193–201 (2002).

<sup>2</sup>H. Raanaei, H. Lidbaum, A. Liebig, K. Leifer, and B. Hjörvarsson, "Structural coherence and layer perfection in Fe/MgO multilayers," *J. Phys.: Condens. Matter* **20**(5), 055212 (2008).

<sup>3</sup>T. Mühge, A. Stierle, N. Metoki, H. Zabel, and U. Pietsch, "Structural properties of high-quality sputtered Fe films on Al<sub>2</sub>O<sub>3</sub> (1120) and MgO(001) substrates," *Appl. Phys. A: Solids Surf.* **59**(6), 659–665 (1994).

<sup>4</sup>B. Lairson, A. Payne, S. Brennan, N. Rensing, B. Daniels, and B. Clemens, "In situ x-ray measurements of the initial epitaxy of Fe (001) films on MgO (001)," *J. Appl. Phys.* **78**(7), 4449–4455 (1995).

<sup>5</sup>C. Li and A. J. Freeman, "Giant monolayer magnetization of Fe on MgO: A nearly ideal two-dimensional magnetic system," *Phys. Rev. B* **43**(1), 780–787 (1991).

<sup>6</sup>Y. Y. Huang, C. Liu, and G. P. Felcher, "Magnetization of ultrathin bcc Fe films on MgO," *Phys. Rev. B* **47**(1), 183–189 (1993).

<sup>7</sup>C. Liu, Y. Park, and S. D. Bader, "Resistance minimum in ultrathin ferromagnetic films of Fe on MgO (100)," *J. Magn. Magn. Mater.* **111**(3), L225–L230 (1992).

<sup>8</sup>S. Yuasa, T. Nagahama, A. Fukushima, Y. Suzuki, and K. Ando, "Giant room-temperature magnetoresistance in single-crystal Fe/MgO/Fe magnetic tunnel junctions," *Nature Mater.* **3**(12), 868–871 (2004).

<sup>9</sup>R. Fan, S. Lee, J. Goff, R. Ward, S. Wang, A. Kohn, C. Wang *et al.*, "The influence of interfacial roughness on the coherence of structure and magnetic coupling across barriers in Fe/MgO multilayers," *J. Phys.: Condens. Matter* **22**, 226004 (2010).

<sup>10</sup>M. Arita, K. Wakasugi, K. Ohta, K. Hamada, Y. Takahashi, and J. Choi, "Microstructure and electric property of MgO/Fe/MgO tri-layer films forming a nano-granular system," *Microelectron. Eng.* **85**(12), 2445–2450 (2008).

<sup>11</sup>M. K. Niranjana, C. G. Duan, S. S. Jaswal, and E. Y. Tsybmal, "Electric field effect on magnetization at the Fe/MgO (001) interface," *Appl. Phys. Lett.* **96**(22), 222504 (2010).

<sup>12</sup>M. Tsujikawa, S. Haraguchi, T. Oda, Y. Miura, and M. Shirai, "A comparative ab initio study on electric-field dependence of magnetic anisotropy in MgO/Fe/Pt and MgO/Fe/Au films," *J. Appl. Phys.* **109**(7), 07C107 (2011).

<sup>13</sup>F. Cebollada, A. Hernando-Mañeru, A. Hernando, C. Martínez-Boubeta, A. Cebollada, and J. González, "Anisotropy, hysteresis, and morphology of self-patterned epitaxial Fe/MgO/GaAs films," *Phys. Rev. B* **66**(17), 1–8 (2002).

- <sup>14</sup>C. Martínez-Boubeta, C. Clavero, J. García-Martín, G. Armelles, A. Cebollada, L. Balcells *et al.*, "Coverage effects on the magnetism of Fe/MgO(001) ultrathin films," *Phys. Rev. B* **71**(1), 13–15 (2005).
- <sup>15</sup>P. Luches, S. Benedetti, M. Liberati, F. Boscherini, I. Pronin, and S. Valeri, "Absence of oxide formation at the Fe/MgO(001) interface," *Surf. Sci.* **583**, 191–198 (2005).
- <sup>16</sup>X.-G. Zhang, W. Butler, and A. Bandyopadhyay, "Effects of the iron-oxide layer in Fe-FeO-MgO-Fe tunneling junctions," *Phys. Rev. B* **68**(9), 6–9 (2003).
- <sup>17</sup>C. Wang, S. Wang, A. Kohn, R. C. C. Ward, and A. K. Petford-Long, "Transmission electron microscopy study of the Fe(001)|MgO(001) interface for magnetic tunnel junctions," *IEEE Trans. Magn.* **43**(6), 2779–2781 (2007).
- <sup>18</sup>C. Tiusan, M. Sicot, M. Hehn, C. Belouard, S. Andrieu, F. Montaigne, and A. Schuhl, "Fe/MgO interface engineering for high-output-voltage device applications," *Appl. Phys. Lett.* **88**(6), 062512 (2006).
- <sup>19</sup>H. Meyerheim, R. Popescu, N. Jedrecy, M. Vedpathak, M. Sauvage-Simkin, R. Pinchaux, *et al.*, "Surface x-ray diffraction analysis of the MgO/Fe(001) interface: Evidence for an FeO layer," *Phys. Rev. B* **65**(14), 1–7 (2002).
- <sup>20</sup>I. Rungger, A. Reily Rocha, O. Mryasov, O. Heinonen, and S. Sanvito, "Electronic transport through Fe/MgO/Fe(100) tunnel junctions," *J. Magn. Mater.* **316**(2), 481–483 (2007).
- <sup>21</sup>F. A. Stevie, C. B. Vartuli, L. A. Giannuzzi, T. L. Shofner, S. R. Brown, B. Rossie *et al.*, "Application of focused ion beam lift-out specimen preparation to TEM, SEM, STEM, AES and SIMS analysis," *Surf. Interface Anal.* **31**(5), 345–351 (2001).
- <sup>22</sup>N. D. Browning, D. J. Wallis, P. D. Nellist, and S. J. Pennycook, "EELS in the STEM: Determination of materials properties on the atomic scale," *Micron* **28**(5), 333–348 (1997).
- <sup>23</sup>F. Cosandey, D. Su, M. Sina, N. Pereira, and G. G. Amatucci, "Fe valence determination and Li elemental distribution in lithiated FeO<sub>0.7</sub>F<sub>1.3</sub>/C nanocomposite battery materials by electron energy loss spectroscopy (EELS)," *Micron* **43**(1), 22–29 (2012).
- <sup>24</sup>P. A. van Aken, V. J. Styras, B. Liebscher, A. B. Woodland, and G. J. Redhammer, "Microanalysis of Fe<sup>3+</sup>/ΣFe in oxide and silicate minerals by investigation of electron energy-loss near-edge structures (ELNES) at the Fe M<sub>2,3</sub> edge," *Phys. Chem. Miner.* **26**(7), 584–590 (1999).
- <sup>25</sup>C. Colliex, T. Manoubi, and C. Ortiz, "Electron-energy-loss-spectroscopy near-edge fine structures in the iron-oxygen system," *Phys. Rev. B* **44**(20), 11402–11411 (1991).
- <sup>26</sup>F. Cosandey, J. F. Al-Sharab, F. Badway, G. G. Amatucci, and P. Stadelmann, "EELS spectroscopy of iron fluorides and FeF<sub>x</sub>/C nanocomposite electrodes used in Li-ion batteries," *Microsc. Microanal.* **13**(2), 87–95 (2007).
- <sup>27</sup>J. Graetz, C. C. Ahn, R. Yazami, and B. Fultz, "An electron energy-loss spectrometry study of charge compensation in LiNi<sub>0.8</sub>Co<sub>0.2</sub>O<sub>2</sub>," *J. Phys. Chem. B* **107**(13), 2887–2891 (2003).
- <sup>28</sup>B. D. Cullity and C. D. Graham, *Introduction to Magnetic Materials*, 2nd ed. (Wiley, Hoboken, N.J., 2009).
- <sup>29</sup>S. Jordan, R. Schad, A. Keen, M. Bischoff, D. Schmooll, and H. van Kempen, "Nanoscale Fe islands on MgO(001) produced by molecular-beam epitaxy," *Phys. Rev. B* **59**(11), 7350–7353 (1999).
- <sup>30</sup>T. Kanaji, T. Kagotani, S. Nagata, "Auger and loss spectroscopy study of surface contamination effect on the growth mode of iron epitaxial films on MgO(001)," *Thin Solid Films* **32**(2), 217–219 (1976).
- <sup>31</sup>G. Fahsold, A. Pucci, and K. H. Rieder, "Growth of Fe on MgO(001) studied by He-atom scattering," *Phys. Rev. B* **61**(12), 8475–8483 (2000).
- <sup>32</sup>M. Siegert and M. Plischke, "Solid-on-solid models of molecular-beam epitaxy," *Phys. Rev. E* **50**(2), 917–931 (1994).
- <sup>33</sup>M. Johnson, C. Orme, A. Hunt, D. Graff, J. Sudijono, L. Sander, and B. Orr, "Stable and unstable growth in molecular beam epitaxy," *Phys. Rev. Lett.* **72**(1), 116–119 (1994).
- <sup>34</sup>Y. Park, E. E. Fullerton, and S. D. Bader, "Growth-induced uniaxial in-plane magnetic anisotropy for ultrathin Fe deposited on MgO(001) by oblique-incidence molecular beam epitaxy," *Appl. Phys. Lett.* **66**(16), 2140 (1995).
- <sup>35</sup>K. Thürmer, R. Koch, M. Weber, and K. Rieder, "Dynamic evolution of pyramid structures during growth of epitaxial Fe(001) films," *Phys. Rev. Lett.* **75**(9), 1767–1770 (1995).
- <sup>36</sup>G. Fahsold, A. Bartel, O. Krauth, and A. Lehmann, "In-situ investigation of Fe ultrathin film growth by infrared transmission spectroscopy," *Surf. Sci.* **433–435**, 162–166 (1999).
- <sup>37</sup>D. Petti, M. Cantoni, C. Rinaldi, S. Brivio, R. Bertacco, J. Gazquez *et al.*, "Sharp Fe/MgO/Ge(001) epitaxial heterostructures for tunneling junctions," *J. Appl. Phys.* **109**(8), 084909 (2011).
- <sup>38</sup>J. L. Vassent, M. Dynna, A. Marty, B. Gilles, G. Patrat, "A study of growth and the relaxation of elastic strain in MgO on Fe(001)," *J. Appl. Phys.* **80**(10), 5727 (1996).
- <sup>39</sup>S. L. Blank and J. A. Pask, "Diffusion of iron and nickel in magnesium oxide single crystals," *J. Am. Ceram. Soc.* **52**(12), 669–675 (1969).
- <sup>40</sup>R. A. Weeks, J. Gastineau, and E. Sonder, "Distribution of Fe<sup>3+</sup> in iron-doped MgO single crystals," *Phys. Status Solidi A*, **61**(1), 265–274 (1980).
- <sup>41</sup>J. M. Coey, *Magnetism and Magnetic Materials* (Cambridge University Press, Cambridge, 2009).
- <sup>42</sup>Y. V. Goryunov, N. N. Garif'yanov, G. G. Khaliullin, I. A. Garifullin, F. Schreiber, T. Mühge *et al.*, "Magnetic anisotropies of sputtered Fe films on MgO substrates," *Phys. Rev. B* **52**(18), 13450–13458 (1995).
- <sup>43</sup>P. Bruno and J.-P. Renard, "Magnetic surface anisotropy of transition metal ultrathin films," *Appl. Phys. A: Solids Surf.* **49**(5), 499–506 (1989).
- <sup>44</sup>H. Matsuda, S. Okamura, T. Shiosaki, H. Adachi, and H. Sakakima, "Magnetic and magnetoresistance properties of spin valves using epitaxial Fe<sub>3</sub>O<sub>4</sub>(110) as the pinning layer," *J. Appl. Phys.* **98**(6), 063903 (2005).
- <sup>45</sup>S. Schnittger, C. Jooss, and S. Sievers, "Magnetic and structural properties of cobalt ferrite thin films and structures," *J. Phys.: Conf. Ser.* **200**(7), 072086 (2010).
- <sup>46</sup>G. Hu, V. G. Harris, and Y. Suzuki, "Microstructure and magnetic properties of cobalt ferrite thin films," *IEEE Trans. Magn.* **37**(4), 2347–2349 (2001).
- <sup>47</sup>J. Camarero, J. J. de Miguel, R. Miranda, and A. Hernando, "Thickness-dependent coercivity of ultrathin Co films grown on Cu(111)," *J. Phys.: Condens. Matter* **12**(35), 7713–7719 (2000).
- <sup>48</sup>M. L. Munford, M. L. Sartorelli, L. Seligman, and A. A. Pasa, "Morphology and magnetic properties of Co thin films electrodeposited on Si," *J. Electrochem. Soc.* **149**(5), C274 (2002).
- <sup>49</sup>A. Moschel, R. Hyman, A. Zangwill, and M. Stiles, "Magnetization reversal in ultrathin films with monolayer-scale surface roughness," *Phys. Rev. Lett.* **77**(17), 3653–3656 (1996).
- <sup>50</sup>C. Chen, O. Kitakami, and Y. Shimada, "Particle size effects and surface anisotropy in Fe-based granular films," *J. Appl. Phys.* **84**(4), 2184 (1998).
- <sup>51</sup>J.-W. Cai, S. Okamoto, O. Kitakami, and Y. Shimada, "Large coercivity and surface anisotropy in MgO/Co multilayer films," *Phys. Rev. B* **63**(10), 1–7 (2001).
- <sup>52</sup>J. Islam, Y. Yamamoto, E. Shikoh, A. Fujiwara, H. Hori, "A comparative study of Co and Fe thin films deposited on GaAs(001) substrate," *J. Magn. Mater.* **320**(3–4), 571–574 (2008).
- <sup>53</sup>D. Sander, A. Enders, J. Kirschner, "Magnetoelastic coupling and epitaxial misfit stress in ultrathin Fe(100)-films on W(100)," *J. Magn. Mater.* **198–199**, 519–521 (1999).
- <sup>54</sup>C. L. Platt, A. E. Berkowitz, D. J. Smith, and M. R. McCartney, "Correlation of coercivity and microstructure of thin CoFe films," *J. Appl. Phys.* **88**(4), 2058 (2000).
- <sup>55</sup>S. K. Chen, F. T. Yuan, and T. S. Chin, "Effect of interfacial diffusion on microstructure and magnetic properties of Cu/FePt bilayer thin films," *J. Appl. Phys.* **97**(7), 073902 (2005).